



Study on the Bond Behavior between the Connection and Hybrid Reinforcement (Steel/FRP Bar) for Precast Concrete Structures

Y. L. Sun⁽¹⁾, Z. Y. Sun^{(2)*}, L. Z. Yao⁽³⁾, A. R. Vatuloka⁽⁴⁾, Y. Wei⁽⁵⁾, G. Wu⁽⁶⁾

⁽¹⁾ School of Civil Engineering, Southeast University, Nanjing 211189, China, sunyl@seu.edu.cn

⁽²⁾ Southeast University, Key Laboratory of Concrete and Prestressed Concrete Structures of the Ministry of Education, Nanjing 211189, China, sunzeyang@seu.edu.cn

⁽³⁾ School of Civil Engineering, Southeast University, Nanjing 211189, China, ylz19881023@126.com

⁽⁴⁾ School of Civil Engineering, Southeast University, Nanjing 211189, China, 185545@seu.edu.cn

⁽⁵⁾ College of Civil Engineering, Nanjing Forestry University, Nanjing 210037, China. Wy78@njfu.edu.cn

⁽⁶⁾ Southeast University, Key Laboratory of Concrete and Prestressed Concrete Structures of the Ministry of Education, Nanjing 211189, China, g.wu@seu.edu.cn

Abstract

Due to the good anti-corrosion performance of an SFCB (Steel-FRP (Fiber-reinforced polymer) Composites Bar), the durability of the fabricated concrete structures caused by construction defects or insufficient connections can be partially solved. A novel grout-filled coupling sleeve named GDPS (Grouted Deformed Pipe Splice) used for deformed rebar connection was selected for SFCB/FRP bar in this paper. Both experimental and numerical study were conducted, the test results were summarized and discussed in terms of typical failure modes, load-slip behaviors, the influence of the bonded length and type of rebar was analyzed. Test results showed that the failure modes and load-slip relationships of connections for SFCB were more diverse than that for the deformed bar, the strength demand of a GDPS connection for SFCB is relatively strict because of the higher ultimate strength. The bonded length of the GDPS connector for an SFCB over $15d_b$ can guarantee the full play of the strength. The finite element model was used to verify the test results, it was found that the stiffness mismatch of grout/FRP interface induces minor differentiation of relative slip in SFCB's connector along the bonded length compared to that of deformed bar connector, and almost 1.1 mm relative slip occurred in the free end of SFCB connector even when the bonded length reached $15d_b$. Finally, qualitative design suggestions for SFCB with GDPS were proposed based on the parametric study through numerical methods.

Keywords: Precast structure; Steel-fiber-reinforced polymer composite bar; Connection; Interface properties; Relative slip distributions



1. Introduction

A precast concrete structure can have the advantages of optimized structure performance, accelerated construction speed, improved labor conditions, and it is expected to become the mainstream structural types [1-3]. Due to the existence of splicing joints/reinforcements, a precast concrete structure has some defects, such as poor integrity, small stiffness or insufficient seismic performance, and the corrosion of the ordinary deformed bar in splicing joints in severe environment such as seaport or chemical industry, may result in an insecure service state [4].

Fiber reinforced polymer (FRP) has the advantages of light weight, high strength and good corrosion resistance, but the disadvantages of low elastic modulus, poor shear strength and high price make it difficult to be widely applied in civil engineering. The damage and durability of a precast concrete structure (mainly beam and columns) can become more controllable and designable through hybrid reinforcement [5-10]. Similar ductility indexes of the FRP-reinforced and steel bar-reinforced beams were verified by Harris and Somboonsong (1998) [5]. A numerical method proposed by Kara for estimating the curvature, deflection and moment capacity of hybrid FRP/steel reinforced concrete beams, and the FRP reinforcement was found to play an important role to resist the increased load after the yielding of steel bar [7]. Numerical study conducted by Sun and Wu (2012) showed that, columns hybrid reinforced by FRP and steel could achieve a smaller residual displacement with lower requirement of the column base curvature as that of the corresponding reinforced concrete (RC) column [10]. Moreover, fatigue flexural and blast responses of concrete beams can be improved by hybrid reinforcement [11,12], for example, Liu and Zhou (2019) carried out an experimental study on blast responses of concrete beams reinforced with steel/GFRP composite bars, results showed that composite bars reduce the plastic deformation and the residual deflection compared with the steel-bar reinforced concrete beams [11].

One of the key issues of a precast concrete structure is its connection technology, and a good connection is the guarantee for the full use of an SFCB/FRP bar. The connection technology for a deformed rebar has been widely studied by researcher and been widely used in engineering, such as full grouting sleeve connection, semi-grouting sleeve connection, screw stirrup anchor lap joint and grouting bellows connection et al. In order to solve the defects of the traditional grouting sleeve connection such as high cost and low corrosion resistance, novel grout splice sleeves such as grouted deformed pipe splice (GDPS sleeve) [13,14] and glass FRP splice sleeve with corrugated (CP-GFRP splice sleeve) [15] were proposed. Zheng and Guo (2016) proposed a novel grout-filled coupling sleeve named as GDPS, and the experimental study conducted by Zheng shows that, according to the Chinese Code JGJ355 [16], the basic effective bonded length of a GDPS connection for a deformed bar was $7d_b$ [14]. However, the study on GDPS connections for FRP bars or SFCBs is currently still lacking.

This paper presents an experimental study on the bond performance of the GDPS connections for SFCBs and basalt FRP (BFRP) bars. The finite element methods (FEM) based on LS-DYNA was discussed to evaluate the bond behavior between SFCB and grout, the failure mechanism and relative slip distributions were also obtained. Finally, parametric analysis about the influence of FRP properties on the bond performance of an SFCB grouting connector were conducted, and the corresponding qualitative design suggestion was proposed.

2. Test Design

2.1 Material properties and details of the GDPS

The splice sleeves were manufactured with a low-alloyed standard seamless steel pipe through cold rolling techniques (Fig. 1), and several outer grooves and inner ribs are rolled on their surfaces, which can improve the bond strength of the interface between the sleeve and inner grout as well as that of the sleeve and surrounding concrete [17]. The outer diameter (D_{out}), inner diameter (D_{in}) and thicknesses (t_g) of the GDPS were 42 mm, 32 mm and 5 mm respectively. Space between ribs (d_{r1} and d_{r2}) are 25 mm and 20 mm



respectively. The lengths of GDPS in this paper consists of 174 mm, 214 mm, 304 mm, 364 mm, 434 mm, and 524 mm. The values were 395 MPa for yield strength, 495 MPa for ultimate strength, 0.0019 for yield strain, 0.051 for ultimate strain and 206 GPa for elastic modulus, respectively.

Grout with high strength and micro-expansion was employed in this study, and the uniaxial compressive strength f_c was measures from standard 3 grout cubes tests (70.7 mm \times 70.7 mm \times 70.7 mm) according to JG/T408-2013 [18]. The corresponding average strength were 66.3 MPa and 87.5 MPa after curing 7 days and 28 days, respectively.

Three kinds of rebars including S10, B49 and S10B49 were selected, and the corresponding surface configurations were presented in Fig. 2. S10 represents deformed rebar with 10 mm nominal diameter refer to GB1499.2-2018 [19], B49 was made of 49 bundles basalt fiber (2400 tex) by pultrusion process, and S10B49 was composed by inner S10 and outer longitudinal 49 bundles basalt fiber [20]. Unlike deformed bars with crescent ribs (Fig. 2 (a)), spiral ribs (Figs. 2 (b) and (c)) of SFCB/BFRP bar were formed by plastic tape during the pultrusion process, averaged spacing were 7.6 mm, and 0.41 mm for the rib's depth, respectively. The outer diameters of B49 and S10B49 were 13.0 mm and 14.6 mm, respectively. Tensile tests on the rebars were conducted according to standard GB/T228.1-2010 and GB/T 30022-2013 [21, 22], and the rebars were cut from the same batch reinforcements as the ones used in the pullout tests. The mechanical test results of all the reinforcements, including the elastic modulus (E), yield strength (f_y), yield strain (ε_y), ultimate strength (f_u) and ultimate strain (ε_u), were summarized in Table 1.

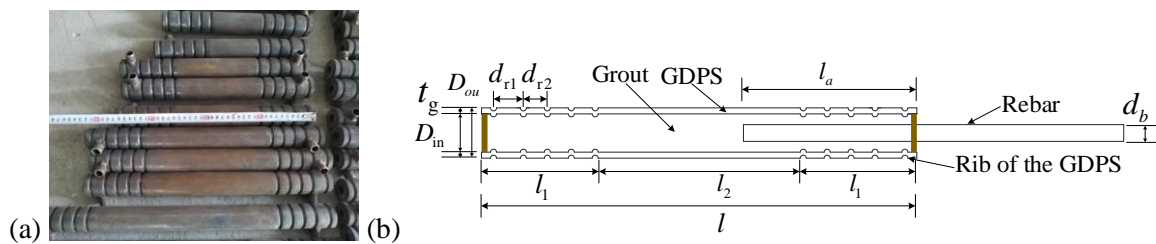


Fig. 1 – Details of the coupler specimens (unit: mm): (a) photos of GDPSs and (b) geometry of a GDPS

Table 1 – Properties of deformed rebar, BFRP bar and SFCB

Specimen	E (GPa)	f_y (MPa)	ε_y	f_u (MPa)	ε_u
S10	200	430	0.002	630	0.12
B49	50	-	-	1130	0.023
S10B49	108	263	0.002	672	0.025

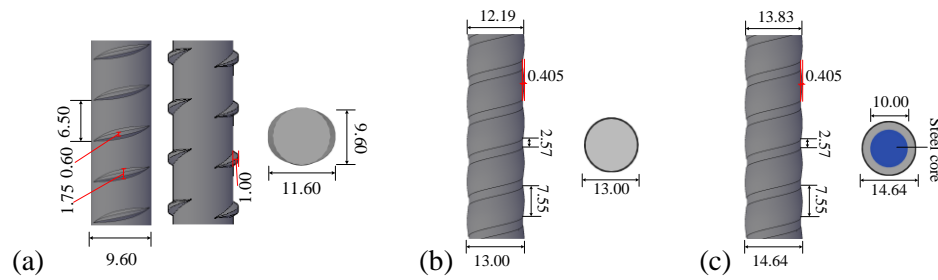


Fig. 2 – Surface configuration of the reinforcement (unit: mm): (a) deformed bar; (b) BFRP bar; (c) SFCB

2.2 Details of the tested specimens

Twenty-four specimens were tested, which were summarized in Table 2. Specimens were divided into 3 groups in accordance with bonded length l_a . The steel bar specimens (S10) were the control specimen used to demonstrate the difference of the bonding performance between FRP and grout. Short bonded length l_a of $5d_b$ [23] (d_b is nominal diameter of the rebars) was selected here to compare with long bonded length l_a of $15d_b$, and moderate l_a of $10d_b$. The symbols “S10-yd-z”, “B49-yd-z” and “S10B49-yd-z” were used for the specimens S10, B49 and S10B49 respectively, where y and z represent the ratio of bonded length to diameter and numbers of replicate specimens, respectively. For example, specimen B49-10d-2 is the 2nd replicate specimen of B49 with l_a of $10d_b$. As illustrated in Fig. 3, the manufacture process of the specimens can be divided into the following four steps: (1) the rebars were cut into a specific length according to the design dimensions; (2) GDPS were placed on a wooden fixture, and rebars were center inserted into GDPS parallel to the longitudinal axis. (3) high-strength grout was injected from the grouting entrance into the sleeve; (4) all specimens were cured for 21 days.

Table 2 – Specimens design

Type of bar	Specimen number	l (mm)	l_a (mm)	P_m (kN)	P_y (kN)	s_m (mm)	s_y (mm)	f_{ust}/f_{syk}	f_{ust}/f_{stk}	Failure mode ^a
S10	S10-5d-1	174	$5d_b$	54.7	47.3	19.7	4.6	1.62	1.23	a
	S10-5d-2			52.2	43.3	20.3	5.0	1.54	1.17	
	S10-7d-1	174	$7d_b$	54.3	44.6	23.2	6.3	1.60	1.22	a
	S10-7d-2	214		51.6	42.4	22.7	5.2	1.53	1.16	
	S10-9d-1	214	$9d_b$	51.7	42.4	20.9	4.6	1.53	1.16	a
	S10-9d-2			54.6	45.7	20.6	5.1	1.62	1.23	
B49	B49-5d-1	174	$5d_b$	62.1	-	7.5	-	-	0.52	b
	B49-5d-3			62.9	-	6.5	-	-	0.53	
	B49-10d-1	304	$10d_b$	121.4	-	15.1	-	-	1.01	b
	B49-10d-2			118.0	-	14.9	-	-	0.98	
	B49-10d-3			123.7	-	15.9	-	-	1.03	
	B49-15d-1	434	$15d_b$	132.2	-	18.4	-	-	1.1	c
	B49-15d-2			144.9	-	22.9	-	-	1.21	



	B49-15d-3			133.1	-	18.9	-	-	1.11	
S10B49	S10B49-5d-1	214	5d _b	63.8	-	7.5	-	1.45	0.63	b
	S10B49-5d-2			72.2	-	7.6	-	1.64	0.71	
	S10B49-5d-3			71.5	-	7.4	-	1.62	0.71	
	S10B49-10d-1	364	10d _b	101.6	42.9	11.5	2.8	2.30	1.00	c
	S10B49-10d-2			108.5	42.6	12.0	2.7	2.45	1.07	
	S10B49-10d-3			104.6	43.7	11.9	3.0	2.37	1.03	
	S10B49-15d-1	524	15d _b	109.4	40.0	17.7	4.0	2.48	1.07	a
	S10B49-15d-2			111.3	43.9	14.2	3.3	2.52	1.10	
	S10B49-15d-3			111.3	43.0	13.9	2.9	2.52	1.10	

^a (a) fracture of rebar; (b) pull-out failure without fracture; (c) mixed failure with both fracture of rebar and large relative slip (pull-out).



Fig. 3 - Manufacture process of test specimens: (a) the reinforcements cut off; (b) centered placed components; (c) grout pouring; (d) curing and hardening of grout

2.3 Test setup

As shown in Fig. 4, the loading support system was a steel framed structure. The pull-out load was applied by a hydraulic actuator with an axial capacity of 500 kN, and transmitted through a welded u-shaped steel groove at the end of the sleeve. The force sensor was installed at the top of the specimen. A displacement extensometer was clamped in the unembedded region of rebar. Axial displacement of the connector was measured by two linear variable displacement transducers (LVDTs), which can reflect the deformation of the loading end. The load was applied under load control with the load rate was 200 N/s at the initial stage, and changed to displacement control when the applied load was relatively large.

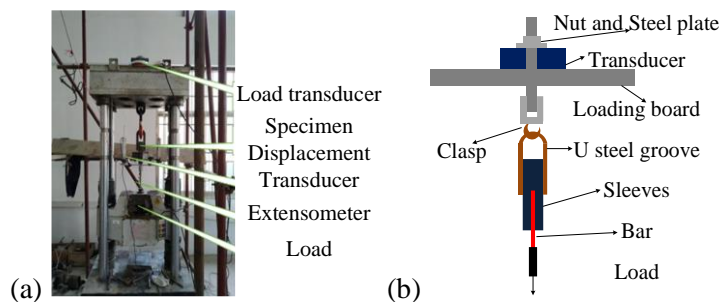


Fig. 4 - Test setup and instrumentation: (a) Photograph of test setup; (b) schematic diagram



3. Experimental results

3.1 Failure modes

Three typical failure modes, namely the fracture of the reinforcement, pull-out failure without fracture and mixed failure with both fracture and large relative slip, were illustrated in Fig. 5. Type S10 specimens all failed with the fracture of rebar (Fig. 4a), its mean that the confinement effect and friction force between steel rebar and grout in case of l_a were enough for the ultimate strength development, thus there was no obvious slip of the free end of the steel bar specimen. However, experimental study conducted by Zhen and Guo [24] showed that slippage between grout and rebar occurred in GDPS coupler with S22 and S25 due to too high strength of rebar in case of bonded length range from $6.9d_b$ to $7.5d_b$. The specimens (B49-5d and S10B49-5d) with short bonded length mainly failed by bar pull-out failure, as shown in Fig. 4(b). This was because of the insufficient bond-shear capacity with too small bond length. The modes of the S10B49 specimens with $10d_b$ bonded length were mainly characterized by the mixed failure with both fracture and pull-out. As the bond length increased to $15d_b$, rupture of the reinforcement occurred, which was caused by the sufficient bond length. It seems like that B49-15d failed with rupture of rebar accompanying bar slip.

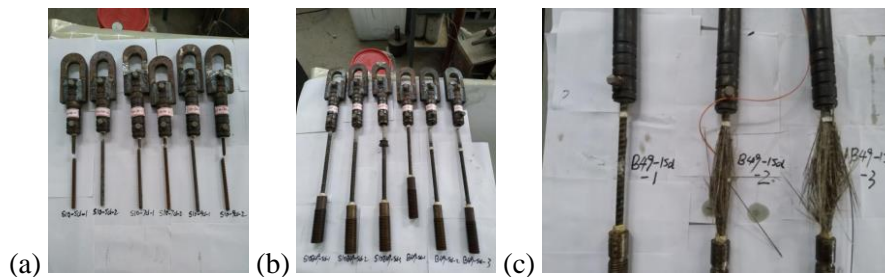


Fig. 5 – Failure modes: (a) fracture of rebar; (b) pull-out failure without fracture; (c) mixed failure with both fracture of rebar and large relative slip (pull-out).

3.2 Load - slip behavior

Fig. 6 presents the load-slip curves of the connectors, divided by rebar type and bonded length. In each figure, the black solid line, black dash line and black dot line is load – slip curve of each replicate specimen, whereas the red solid line represents the numerical result. The load-slip (loaded end) curves of S10 specimens showed the elastic, yielding, hardening and tightening regions that similar to those for steel bars under uniaxial tension [25] (Figs. 6 (a) – (c)). B49 and S10B49 specimens anchored with the shorter length ($5d_b$) showed an initially linear response, followed by a decreased stiffness up to the peak load and a post-peak pseudo-ductile softening branch (Figs. 5 (d) and (h)). For specimens S10B49 with bonded length of $10d_b$ and $15d_b$, the load-slip curves presented as typical four-region curves (Figs. 6 (i) and (j)), featuring a bilinear region, pseudo-ductile softening and a residual strength region. In the bilinear region, the stiffness turning point represents for the yield of inner steel bar. In the post-yield stage, the load capacity decreased sharply, which was associated with rupture of outer basalt fiber. In the residual strength region, if the outer FRP ruptured, the load capacity stayed at a specify value dominated by hardening of inner steel.

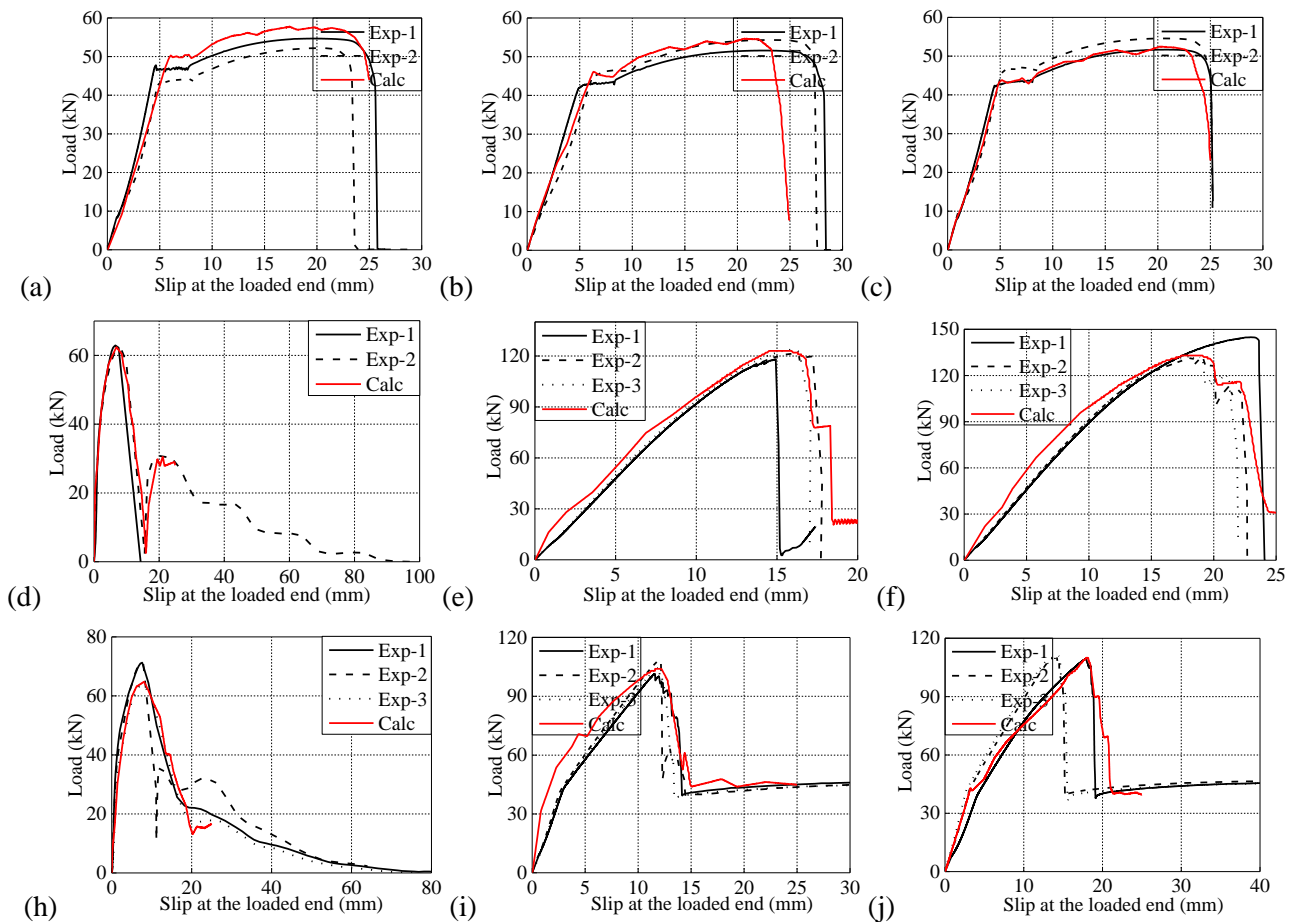


Fig. 6 – Load – Slip curves of specimens: (a) S10-5d; (b) S10-7d; (c) S10-9d; (d) B49-5d; (e) B49-10d; (f) B49-15d; (h) S10B49-5d; (i) S10B49-10d; (j) S10B49-15d

3.3 Performance of GDPS sleeve

The feasibility of GDPS for connection of steel bar has been confirmed by Zheng et al. [13,14] through extensive experimental and theoretical analysis, but the application of GDPS for SFCB is still unknown. Based on JGJ107 [26], the ultimate tensile strength of the splice can be classified into three grades, as illustrated in Table 3, and corresponding scopes of application were specified. In Table 3, f_{ust} , f_{stk} and f_{syk} represents ultimate tensile strength of splice, specified standard tensile strength of connected bar and specified standard yield strength of connected bar respectively, and f_{ust} was calculated by $4P_m/\pi d_b^2$. Grade I or II splice should be used in concrete structures where required high strength and ductility of rebar, and Grade I splice should be selected when percentage of connected rebar area up to 100% in the same member section. Grade III splice can be used in the parts of the concrete structures where the rebar stress is high but with lower ductility requirements.

It can be seen from Table 2 that the GDPS was suitable for the connection of BFRP bar and SFCB in case of bonded length of $15d_b$, and it's worth been noted that B49 type coupler meets $f_{ust} \geq 1.1f_{stk}$ (connector damage) while S10B49 type connector meets $f_{ust} \geq 1.0f_{stk}$ (fracture of splice bar). Which means that the basic effective length of SFCB type GDPS connector is twice as much as that of deformed bar type coupler. Compared to energy dissipation caused by yield of deformed bar, the reparability or seismic resilience of an SFCB reinforced concrete structure is mainly related to the post-yield stiffness (stress hardening) instead of ductility. Thus, further work aimed at optimization of grouting sleeve with minimum basic anchor length that make full use of the strength, ductility and secondary stiffness of SFCB urgently needs to be conducted.



Table 3 – Strength grades of splice

Strength grade	I	II	III
Ultimate tensile strength (f_{ust})	$f_{ust} \geq f_{stk}$ (fracture of splice bar) $f_{ust} \geq 1.1f_{stk}$ (connector damage)	$f_{ust} \geq f_{stk}$	$f_{ust} \geq 1.25f_{syk}$
Scope of application	Allowing 100% connection in cross sections of the specify member	Allowing 50% connection in cross sections of the specify member	Avoiding application in joint area with dense stirrup reinforced of frame beam end and column end

4. Numerical analysis

4.1 Finite element model

An analysis was carried out by a nonlinear explicit dynamic FE package (ANSYS/LS-DYNA) for the numerical simulation of the quasi-static pull-out test of GDPS connector. The solid 164 eight-node element was utilized for modeling the GDPS, deformed rebar, BFRP and grout components. The model configuration was shown in Fig. 7, the boundary condition of the coupler is fixed support at end of GDPS (free end in the test) and the load was applied by displacement with 100 mm/s.

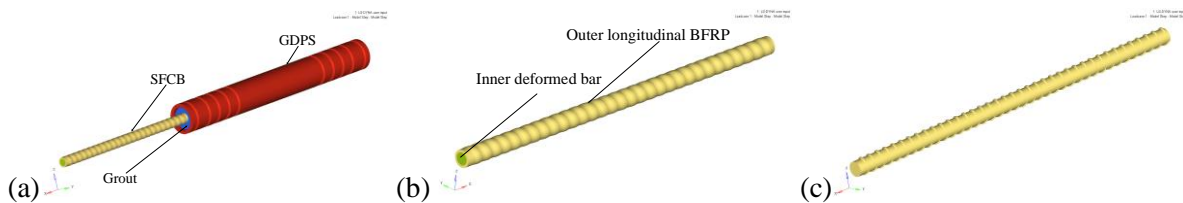


Fig. 7 - FEM models: (a) specimen S10B49-15d; (b) component SFCB; (c) component deformed bar

The material model #111 *MAT_JOHNSON_HOLMQUIST_CONCRETE [27] was used to simulate the connector grout, this model can be used for cement-based material such as concrete subjected to large strains and high pressures. The equivalent strength is expressed as a function of the pressure, strain rate, and damage. The material model #22 *MAT_COMPOSITE_DAMAGE was used to simulate the BFRP, which can be used for both shell element and solid element, and Tsai-Wu failure criteria [28,29] suggested by Chang was adopted in this model. The elastic-plastic materials model #24 *MAT_PLASTIC_KINEMATIC was employed to simulate the GDPS and rebar.

The contact and sliding at the interfaces between grout and reinforcement element is a key issue in FE modeling in this paper, especially for problems involving both large deformation and material nonlinearity. The contact algorithm *CONTACT_AUTOMATIC_SURFACE_TO_SURFACE was selected for the contact between grout and bar, friction coefficient exponential decay model which assumed that friction factor μ_c associated with interface relative velocity was adopted. Parameters of the ASTS model shown in Table 4. F_S , F_D and D_C represents the coefficient of static friction, coefficient of dynamic friction, and exponential decay coefficient, respectively. To avoid the volatility and dispersion of the explicit solution process, viscous damping coefficient $V_{DC} = 0.28$ was adopted. Considering the complexity and nonlinearity of contact, search depth, pinball segment based contact and warped segment checking were used here.



Table 4 - Details parameters of ASTS contact

F_S	F_D	D_C	V_{DC}	DEPTH	SBOPT	SOFT
0.51	0.2	63	0.28	5	3	2

4.2 Model validation and discussion

Fig. 6 shows comparison of the load-slip curves between experimental and numerical results. Generally, numerical models can correctly simulate the ultimate load, pseudo-ductile softening and slip process. For S10 specimens, the largest variation between numerical and experimental results in s_y was 29%, which occurred in specimen S10-5d. For specimens B49 and S10B49, the largest variation occurred in P_m was 3% and 6%, respectively. The analytical and experimental results indicate that the proposed numerical methods can conservatively estimate the actual ultimate axial load of the novel connector for the composite bars under pull-out loading with an average underestimation of 3.0%.

4.3 Distribution of relative slip

The relative slip between the reinforcement and grout can be calculated by Eq. (1):

$$s(x) = u_s(x) - u_c(x) \quad (1)$$

where $u_s(x)$ and $u_c(x)$ represents the calculated absolute displacement of rebar and grout, respectively. Distributions of relative slip were shown in Fig. 8, and Fig. 9 were the corresponding nephograms. Basically, at the same load level, $s(x)$ in the case of shorter bonded length is generally higher than that of specimens with longer bonded length, which is reasonable that the shorter bonded length means lower shear stiffness to resist relative slippage [30]. The relative slip between SFCB and grout in case of shorter anchor length is linear decreased, while nonlinear degradation occurred in specimens with longer bonded length. Moreover, differentiation of $s(x)$ changed slightly as the load increases, for example, there was only 6.6% variation between loaded end and free end when the load reached the peak load for S10B49-5d while that of 53% for specimen S10B49-15d. It can be explained that, the connector with shorter bonded length means more fully shear stress development than that of longer anchored length. Finally, relative slip $s(x)$ up to 1.05 mm happened even when the bonded length reached $15d_b$, which may seriously affect the serviceability of a precast SFCB reinforced concrete structure.

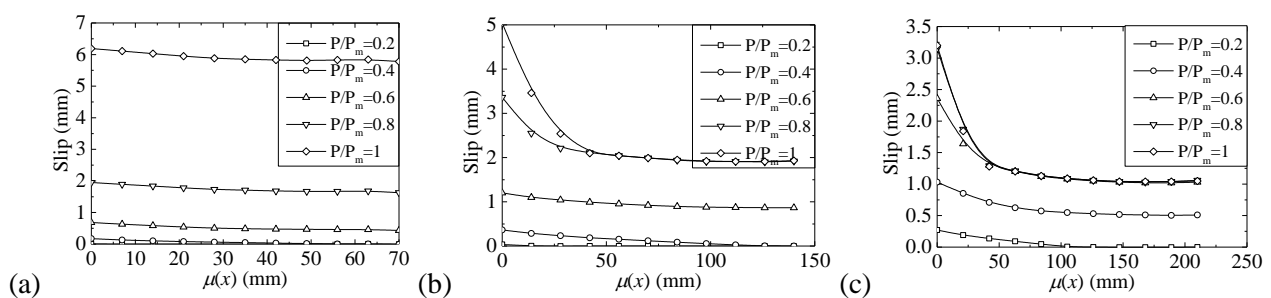


Fig. 8 - Distribution of relative slip under pull-out loading: (a) S10B49-5d; (b) S10B49-10d; (c) S10B49-15d

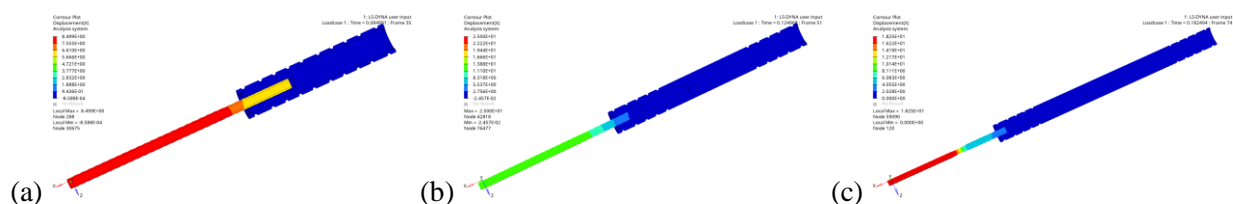


Fig. 9 – Numerical nephograms of the absolute displacement: (a) S10B49-5d; (b) S10B49-10d; (c) S10B49-15d



4.4 Parametric Study

Based on the above experimental and exploratory numerical study, it can be concluded that the pull-out performance of GDPS connections for SFCBs was more diverse than that of deformed bars. In order to investigate the influences of shear modulus of SFCB's outer FRP on the behavior of GDPS connections for SFCB, a parametric analysis was conducted. The numerical results including ultimate load P_m and the corresponding slip s_m were analyzed.

Fig. 10 shows the influence of the shear modulus of BFRP on the ultimate load and the corresponding slip, all the dimensions of the connector were equal to those of the tested specimens S10B49-5d. Four different shear modulus (ranging from 10 GPa to 90 GPa) of BFRP were adopted in the FEM model. It can be found from Fig. 10 that, the P_m of a BFRP connector with shear modulus 90 GPa was 6%, 6% and 1% larger than that with 10 GPa, 30 GPa and 60 GPa shear modulus, respectively. The corresponding relative slip reduced by 1.1%, 0.6% and 0.6%, respectively. Hence, the increased shear modulus can increase the P_m while little effect on the corresponding interface relative slip, this was caused by the larger prying and wedging action produced by the rougher surface of SFCB/grout. Based on the above parametric study, it can be speculated that the mutual matching of BFRP anisotropy stiffness and SFCB's rib geometry was a key factor for the pull-out performance of a SFCB grouting anchorage.

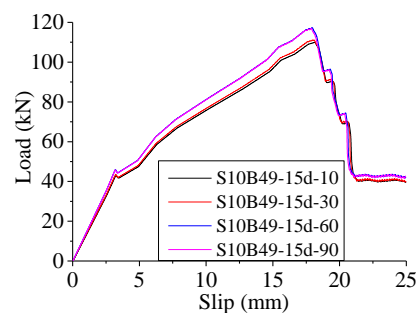


Fig. 10 - Comparison of results for connector with different parameters

5. Conclusions

An experimental and numerical investigation on the pull-out behavior of the novel GDPS connector for SFCB were conducted in this paper. The main conclusions were as follows:

1). The failure modes of the GDPS connector for BFRP bar and SFCB can be characterized by fracture of the bonded reinforcement, pull-out failure without fracture and mixed failure with both fracture and large relative slip (pull-out). The specimens with shorter bonded length ($5d_b$) mainly failed by pull-out failure, mid-long bonded ($10d_b$) specimens occurred mixed failure with both fracture and large relative slip, and longer bonded ($15d_b$) specimens mainly failed by rupture of rebar.

2). Generally, the load-slip curves show an initially linear increase response, followed by a stiffness nonlinear reduction up to the peak load in case of shorter anchored length ($5d_b$), until load sharp decline (pull out). Specimens of mid-long and longer bonded length featuring a bilinear region, pseudo-ductile softening and a residual strength region. GDPS was suitable for the connection of SFCB in case of bonded length of $15d_b$, and basic effective length of SFCB type GDPS connector is twice as much as that of deformed bar type coupler.

3). Proposed numerical model can conservatively estimate the ultimate pull-out load of the connector for SFCB with an average underestimation of 3.0%. Minor differentiation about slip decay along bonded length, mainly caused by the stiffness mismatch of grout/FRP interface, and approximately 1.1 mm relative occurred in free end of SFCB GDPS connector even when the bonded length reached $15d_b$, which may seriously affect the serviceability states of an SFCB reinforced precast structure.



4). Parametric study shows that changing shear stiffness of BFRP can effectively improve the ultimate pull-load by 6%, whereas it has little effect on the corresponding relative slip. Mutual matching of BFRP's anisotropy stiffness and rib geometry can optimize the bond performance of GDPS connection technology for SFCB.

6. Acknowledgements

The authors would like to acknowledge financial support from the National Key Research and Development Program of China (2016YFC0701100), the National Natural Science Foundation (Grant Nos. 51778130 and 51525801), and the Fundamental Research Funds for the Central Universities, Southeast University.

7. References

- [1] Ericson AC (1994): Emulation design of precast concrete. *The Construction Specifier*, **47**(10), 96-103.
- [2] Khare R, Maniyar MM, Uma S (2011): Seismic performance and design of precast concrete building structures: An overview. *Journal of Structural Engineering*, **38**(3), 30-33.
- [3] ACI 550.1R09 (2009): Emulation cast-in-place detailing in precast concrete structures. ACI-ASCE Committee 550.
- [4] Kurama YC, Sritharan S, Fleischman RB (2018): Seismic-Resistant precast concrete structure: State of the Art. *Journal of Structural Engineering*, **144**(4), 03118001.
- [5] Harris HG, Somboonsong W, Ko FK (1998): New ductile hybrid FRP reinforced bar for concrete structures. *Journal of Composites for Construction*, **2**(1), 28-37.
- [6] Lau D, Pam HJ (2010): Experimental study of hybrid FRP reinforced concrete beams. *Engineering Structures*, **32**, 3857-3865.
- [7] Kara IF, Ashour AF, Köroğlu MA (2015): Flexural behavior of hybrid FRP/steel reinforced concrete beams. *Composite Structures*, **129**, 111-121.
- [8] Sun ZY, Fu LC, Feng DC, (2019): Experimental study on the flexural behavior of concrete beams reinforced with bundled hybrid steel/FRP bars. *Engineering Structures*, **197**, 109443.
- [9] Ibrahim AI, Wu G, Sun ZY, et al (2017): Cyclic behavior of concrete columns reinforced with partially unbonded hybrid. *Engineering Structures*, **131**, 311-323.
- [10] Sun ZY, Wu G, Wu ZS, et al (2012): Numerical study on seismic performance of concrete columns reinforced by steel-FRP composite bars. *China Civil Engineering Journal*, **45**(5), 93-103. [in Chinese].
- [11] Liu SF, Zhou YZ, Zheng Q (2019): Blast responses of concrete beams reinforced with steel-GFRP composite bars. *Structures*, **22**, 200-212.
- [12] Xu JJ, Zhu P, Ma GZ (2019): Fatigue flexural analysis of concrete beams reinforced with hybrid GFRP and steel bars. *Engineering Structures*, **199**, 109635.
- [13] Zheng YF, Guo ZX, Zhang X (2018): Effect of grout properties on bond behavior of pipe splice. *KSCE Journal of Civil Engineering*, **22**(8), 2951-2960.
- [14] Zheng YF, Guo ZX, Xie M (2015): Pull-out Bond Properties of grouted-filled mechanical splice for Precast concrete construction. *Advanced Materials Research*, **30**, 1078-1081.
- [15] Zhao CF, Zhang ZD, Wang JF (2019): Numerical and theoretical analysis on the mechanical properties of improved CP-GFRP splice sleeve. *Thin-Walled Structures*, **137**, 487-501.
- [16] JGJ355 (2015): Technical specification for grout sleeve splicing of rebars. Beijing, China: China Architecture and Building Press. [in Chinese].



- [17] Zheng YF, Guo ZX (2014): An experimental study of new Grouted Deformed pipe splice under incremental tensile load. *Proceedings of the Thirteenth International symposium on structural Engineering (CPCI)*, Hefei, Anhui, China.
- [18] JG/T408 (2013): Cementitious grout for coupler of rebar splicing. Beijing, China Architecture and Building Press. [in Chinese].
- [19] GB/T1499.2 (2018): Steel for the reinforced of concrete-Part 2: Hot rolled ribbed bars. China Architecture and Building Press. [in Chinese].
- [20] Sun ZY (2013): Seismic behavior and design method of concrete columns reinforced by steel-fiber reinforced polymer composites bars. *Doctor thesis*, Nanjing, China. [in Chinese].
- [21] GB/T228.1 (2010): Metallic materials-tensile testing-Part 1: Method of test at room temperature. China National Standardization Administration. [in Chinese].
- [22] GB/T 30022 (2013): Test method for basic mechanical properties of fiber reinforced polymer bar. China Architecture and Building Press, 2010 [in Chinese].
- [23] Guo ZH (2013): *Reinforced concrete theory*. Tsinghua University Press, 3rd edition. [in Chinese].
- [24] Zheng YF, Guo ZX (2016): Experimental study and finite element analysis on behavior of deformed grout-filled pipe splice. *Journal of Building Structures*, **37**(3), 94-102.
- [25] Lu ZW, Huang Jun, Li YB, et al (2019): Mechanical behavior of grout sleeve splice under uniaxial tensile loading. *Engineering Structures*, **186**, 421-435.
- [26] JGJ107 (2016): Technical specification for mechanical splicing of steel reinforced bars. China Architecture & Building Press. [in Chinese].
- [27] Holmquist TJ, Johnson GR (2011): A Computational Constitutive Model for Glass Subjected to Large Strains, High Strain Rates and High Pressures. *Journal of Applied Mechanics*, **78**(5), 1-9.
- [28] Chang FK, Chang KY (1987): A progressive damage model for laminated composites containing stress concentrations. *Journal of composites materials*, **21**(9), 834-855.
- [29] Chang FK, Chang FY (1987): Post-failure analysis of bolted composites joints in tension or shear-out mode failure. *Journal of composites materials*, **21**(9), 809-833.
- [30] Ling ZB, Yang HF, Liu WQ, et al (2018): Local bond stress-slip relationships between glue laminated timber and epoxy bonded-in GFRP rod. *Construction and Building Materials*, **170**, 1-12.